의학박사 학위논문

Predicting Response for Pharmacotherapy Using Neuroanatomical Single-Subject Pattern Recognition in Obsessive-Compulsive Disorder

강박증 환자에서 대뇌 피질 두께를 이용한 약물 치료반응 예측모델의 구축

2016년 2월

서울대학교 대학원

ABSTRACT

Background: Primary pharmacotherapy regimen for obsessive-compulsive disorder (OCD) named Serotonin reuptake inhibitors (SRIs) does not attain sufficient symptom improvement in 40-60% of OCD. We aimed to decode the differential profile of OCD-related brain pathology per subject in the context of cortical surface area (CSA) or thickness (CT)-based individualized structural covariance (ISC) and to demonstrate the potential of which as a biomarker of treatment response to SRI-based pharmacotherapy in OCD using the support vector machine (SVM).

Methods: T1-weighted magnetic resonance imaging was obtained at 3T from 56 unmedicated OCD subjects and 75 healthy controls (HCs) at baseline. After 4 months of SRI-based pharmacotherapy, the OCD subjects were classified as responders (OCD-R, $N=25$; $\geq 35\%$ improvement) or nonresponders (OCD-NR, $N=31$; $<35\%$ improvement) according to the percentage change in the Yale-Brown Obsessive Compulsive Scale total score. Cortical ISCs sustaining between-group difference ($p < .001$) for every run of leave-one-out group-comparison were packaged as feature set for group classification using the SVM.

Results: An optimal feature set of the top 12 ISCs including a CT-ISC between the dorsolateral prefrontal cortex versus precuneus, a CSA-ISC between the anterior insula versus intraparietal sulcus, as well as perisylvian area-related ISCs predicted the initial prognosis of OCD as OCD-R or OCD-NR with an accuracy of 89.0% (sensitivity 88.4%, specificity 90.1%). Extended sets of ISCs distinguished the OCD subjects from the HCs with 90.7-95.6% accuracy (sensitivity 90.8-96.2%, specificity 91.1-95.0%).

Conclusion: We showed the potential of cortical morphology-based ISCs, which reflect dysfunctional cortical maturation process, as a possible biomarker that predicts the clinical treatment response to SRI-based pharmacotherapy in OCD.

Keywords: obsessive-compulsive disorder; pharmacotherapy; treatment response; structural covariance network; support vector machine

Student Number: 2012-31126

CONTENTS

LIST OF TABLES

LIST OF FIGURES

LIST OF ABBREVIATIONS

ACC: Anterior cingulate cortex

AI: Anterior part of the insular

CBT: Cognitive behavioral therapy

CMF: Correlative morphological feature

CSA: Cortical surface area

CSA-ISC: Cortical surface area-based individualized structural covariance

CSF: Cerebrospinal fluid

CT: Cortical thickness

CT-ISC: Cortical thickness-based individualized structural covariance

dACC: Dorsal part of the anterior cingulate cortex

DAN: Dorsal attention network

DLPFC: Dorsolateral prefrontal cortex

DMN: Default mode network

DSM-IV-TR: Diagnostic and Statistical Manual of Mental Disorders, 4th Edition-Text Revision

EC: Eigenvector centrality

ECN: Executive control network

GM: Grey matter

HAM-A: Hamilton Anxiety Rating Scale

HAM-D: Hamilton Rating Scale for Depression

HC: Healthy control

IPL: Inferior parietal lobule

IPS: Intraparietal sulcus

ISC: Individualized structural covariance

MCC: Middle cingulate cortex

MCI: Mild cognitive impairment

MRI: Magnetic resonance imaging

OCD: Obsessive-Compulsive Disorder

OCD-NR: Obsessive-Compulsive Disorder treatment nonresponder

OCD-R: Obsessive-Compulsive Disorder treatment responder

OFC: Orbitofrontal cortex

PCC: Posterior cingulate cortex

ReHo: Regional homogeneity in the functional connectivity network

ROI: Region-of-interest

SN: Salience network

SNR: Signal-to-noise ratio

SRI: Serotonin reuptake inhibitor

SVM: Support vector machine

T1WI: T1-weighted magnetic resonance image

vACC: Ventral part of the anterior cingulate cortex

WM: white matter

Y-BOCS: Yale–Brown Obsessive–Compulsive Scale

I. INTRODUCTION

1. Pathophysiological Circuit of Obsessive-Compulsive Disorder

Subjects with obsessive-compulsive disorder (OCD) constitute 2-3% of the population worldwide (Fineberg et al., 2007, Hollander, 1997). These individuals repetitively strive against intrusive obsessive thoughts accompanied by compulsive behaviors that provide transient relief from symptom-related distress (Pauls et al., 2014, Ruscio et al., 2010). Previous neuroimaging studies on OCD have reported morphological or functional derangement of multiple brain regions, such as the orbitofrontal cortex (OFC), anterior cingulate cortex (ACC), insula, inferior parietal lobule (IPL), precuneus, superior temporal cortex and lingual cortex, which collectively constitute the pathophysiological brain circuit of OCD called the 'cortico-striato-thalamo-cortical' loop (Fallucca et al., 2011, Pauls et al., 2014, Shaw et al., 2014).

2. Treatment Response in Obsessive-Compulsive Disorder

In response to primary OCD treatment, which consisted of serotonin reuptake inhibitors (SRIs)–based pharmacotherapy with or without cognitive behavioral therapy (CBT) (Pauls et al., 2014), the brain metabolism or morphometry of subjects revealed diverse response patterns in various brain regions (Han et al., 2011, Shin et al., 2014, Yoo et al., 2007). These findings raise the possibility of predetermined treatment response of each OCD patient based on their differential profile of OCD-related brain

pathology. Considering the need for high-dose and long-term use of SRIs as well as a time lag of at least 8-12 weeks before the emergence of initial meaningful symptom improvement in OCD, the earlier identification of individuals who are less likely to exhibit a full response to SRI treatment, *i.e.,* about 40-60% of OCD patients, is crucial for minimizing exposure to ineffective medication and for planning more optimized interventions (Dold et al., 2013, Shim et al., 2011, Stein et al., 2012).

3. Individualized Cortical Structural Covariance

The coordinated variation in brain morphological features including cortical surface area (CSA) or thickness (CT) among brain structures anatomically or functionally interconnected to one another is referred to as the structural covariance (He et al., 2008). A graph theory approach that defined the brain as an integrated complex system rather than a collection of separate, independently operating regions demonstrated that structural covariance describes a small-world network mainly composed of interconnected hubs that participate in multiple modular communities across the network to organize the overall brain network (Binnewijzend et al., 2014, He et al., 2008). Specifically, the high phenotypic covariance of brain morphology among several brain areas could be interpreted as evidence supporting the existence of coordinated neurodevelopmental, maturational and evolutionary processes in the mammalian brain (Alexander-Bloch et al., 2013a, Alexander-Bloch et al., 2013b, Chen et al., 2012). Overcoming the shortcomings of inter-individual cortical structural covariance (which can be difficult to interpret at the individual level), the newer concept of intra-individual cortical thickness-based structural covariance, referred to as 'correlative

morphological feature (CMF)', was recently introduced (Wee et al., 2013). This method successfully outperformed individual ROI-based cortical morphometric statistics in distinguishing subjects with Alzheimer's dementia or mild cognitive impairment from healthy controls (HCs) using the support vector machine (SVM) platform (Wee et al., 2013). Moreover, the dual cortical morphological features of CSA and CT in the context of individualized structural covariance (ISC) enable us to decode not only the disease-related brain changes but also the inherent sensitivity to pharmacotherapy in psychiatric disorders into the primal profile of brain cortical connectome per subject (Chen et al., 2013, Kremen et al., 2013, Meyer et al., 2014, Song et al., 2015).

4. Support Vector Machine

The multivariate pattern recognition algorithm of SVM uses several explanatory features selected from magnetic resonance imaging (MRI) data simultaneously to classify subjects with various psychiatric disorders (including dementia, schizophrenia, bipolar disorder, and OCD) from HCs and to predict the treatment response or clinical prognosis of subjects with MCI, mood disorders or panic disorder, as well as those who are at a high clinical risk for psychosis (Hahn et al., 2014, Hoexter et al., 2013, Koutsouleris et al., 2009, Li et al., 2014, Wee et al., 2013). The SVM has emerged as a powerful supervised learning algorithm with a wide range of biomedical applications because it is able to learn to categorize complex, high-dimensional training data and to generalize the learned classification rules for unseen data, allowing the generation of complex solutions for group classifications and predictions (Noble, 2006).

5. Aim of the Study

To the best of our knowledge, however, no prior studies have reported an SVM-based prediction of the treatment response to pharmacotherapy for OCD. Therefore, in this study, we investigated the neural correlates of the response to SRI-based pharmacotherapy in subjects with OCD using an SVM classification model constructed using both CSA-ISC and CT-ISC. We also aimed to elucidate the use of the optimum group classifier called 'neuroanatomical decision function,' which provides the most accurate prediction of the treatment response of subjects with OCD while differentiating subjects with OCD from HCs.

II. MATERIALS AND METHODS

1. Participants and Clinical Assessments

This study recruited 56 medication-free OCD patients who met the Diagnostic and Statistical Manual of Mental Disorders, 4th Edition-Text Revision (DSM-IV-TR) criteria for OCD as a major Axis I psychiatric disorder from the OCD clinic at Seoul National University Hospital (SNUH) between May 2010 and April 2014. Of the 56 medication-free subjects with OCD, 16 had never been prescribed psychotropic medication, and the remaining 40 subjects had been free of psychotropic medication for at least 4 weeks before entering the study (Berney et al., 2011).

For each subject with OCD, certified psychiatrists scored the Yale–Brown Obsessive–Compulsive Scale (Y-BOCS) (Goodman et al., 1989), Hamilton Rating Scale for Depression (HAM-D) (Muller and Dragicevic, 2003), and Hamilton Anxiety Rating Scale (HAM-A)(Bruss et al., 1994) to measure the severity of their obsessive-compulsive symptomatology and to evaluate the extent of their accompanying depressive mood and anxiety. In addition, 75 HCs (matched with the OCD subjects in terms of age, sex, and years of education) were recruited using advertisement and then were interviewed using the Structured Clinical Interview for DSM-IV-TR Axis I Disorders, Non-Patient Edition to exclude subjects with a history of or current psychiatric disorders from the HC group.

For both the OCD subjects and HCs, additional exclusion criteria included a lifetime history of significant head injury, a seizure disorder, or mental retardation. This study

was approved from the Institutional Review Board of SNUH. After providing a complete description of the study to the subjects, written informed consent was obtained from each subject before study inclusion and all experiments on human subjects were conducted in accordance with the Declaration of Helsinki.

2. Treatment Schedule and Follow-Up

After completing the clinical assessments and baseline MRI, all subjects with OCD underwent outpatient SRI-based pharmacotherapy treatment prescribed in accordance with the clinical decision of psychiatrists at SNUH. None of the 56 OCD subjects were engaged in psychoanalytic psychotherapy or CBT during the initial 4-month period of pharmacotherapy. After the initial 4 months of SRI-based pharmacotherapy, all of the subjects with OCD underwent a clinical re-evaluation consisting of the Y-BOCS, HAM-D, and HAM-A, which were scored by certified psychiatrists. Based on the percentage change in the Y-BOCS total score after the 4 months, the subjects with a Y-BOCS total score improvement $\geq 35\%$ were classified as 'responders,' and all the other subjects were classified as 'nonresponders'(da Conceicao Costa et al., 2013, Dold et al., 2013, Farris et al., 2013).

3. Image Acquisition, Preprocessing and Extraction of Cortical Surface Area and Cortical Thickness Values

Whole-brain anatomy was measured for all subjects using high-resolution T_1-

weighted, three-dimensional Magnetization Prepared Rapid Gradient Echo (TR = 670 ms; TE = 1.89 ms; FOV = 250 mm; FA = 9°; voxel size = 1 × 1 x 1 mm^3) scans on a 3-Tesla scanner (Siemens Magnetom Trio, Erlangen, Germany).

CSA and CT were estimated using FreeSurfer software suite (version 5.3.0, http://surfer.nmr.mgh.harvard.edu; Fischl et al., 2004). The 'recon-all' function of the FreeSurfer suite preprocessed the T1-weighted magnetic resonance imaging (MRI) data within the pipeline consisted of intensity normalisation, registration to Talairach space, skull stripping, tissue segmentation, tessellation of the white matter (WM) boundary, smoothing of the tessellated surface and automatic topology correction (Clarkson et al., 2011). Subsequently, surface deformation processing to define the boundary between WM and pial tissue using the previously tessellated surface as a reference, enabled measurement of CT, calculated as the shortest distance between gray/white matter boundary and the gray matter/CSF boundary at each vertex on the tessellated surface [Fischl and Dale, 2000]. After preprocessing of MRI image completed, automatic parcellation with subsequent extraction of the CSA for the 148 regions of interest (ROI) that comprises the 2009 Destrieux atlas was performed (Destrieux et al., 2010).

The signal-to-noise ratio (SNR) of grey-to-white matter for each T1WI MRI data [calculated using the 'wm-anat-snr –s' command] and of grey matter (GM) intensity for each ROIs of *2009 Destrieux* atlas [measured using the 'mri_segstats –snr' command] demonstrated relative homogeneity of T1WI acquisition quality and of regional SNR across *cortical ROIs*. After thorough visual inspection of the final processed brain images using the *tkmedit* and *tksurfer* for tissue segmentation, surface reconstruction and cortical parcellation (with no significant errors detected in any of the subjects), automatically computed CSA and CT values were then extracted and used to calculate

ISC networks.

4. Graph Theory Approach for Cortical Thickness-Based Correlative Morphological Features: Small-World and Scale-Free Network

Firstly, to investigate the small-world network-related hierarchical nature of cortical thickness-based structural covariance at the individual level, we used the notion of CMF (Wee et al., 2013). The cortical thickness values were z-scored using the mean and standard deviation values of cortical thickness per each individual. Then, the relative intra-individual cortical morphological similarities between various ROIs were computed as $CMF(i,j)=1/e\left((n(i)-n(j))^2\right)$, where $n(i)$ and $n(j)$ denoted the z-scored cortical thickness of the i^{th} and j^{th} ROIs, respectively (Wee et al., 2013). The resulting 148 x 148 matrix (containing a total of 10,878 CMFs per individual; **Figure 1(A)**) was then converted into several binary adjacency matrices with a range of sparsity thresholds (*K;* the ratio of network edges (CMFs) retained as stronger CMFs among all the possible node (ROI) pairs), for use in subsequent graph theoretical analyses (Rubinov and Sporns, 2010).

In graph theory, the global topology of the network-defining small-world organization can be quantified as the characteristic path length (*L;* the average shortest number of steps along the routes of cortical thickness similarity between all pairs of nodes), the clustering coefficient (*C;* the degree of inter-connectedness in local networks consisting of direct neighbors of each node), and the modularity (*Q;* a

quantitative parameter for modular organization of a network) (Newman, 2006; Watts and Strogatz, 1998). To compare these global topology measures of the network across studies, we normalized them as the ratios between the original value and the reference value calculated from the mean global topology of 1,000 random networks that retained the same nodal degree distribution as their original network (Maslov and Sneppen, 2002). Finally, a measurement of small-worldness (*sigma)* was computed as the ratio of normalized *C* (*gamma)* to normalized *L* (*lambda*) (Uehara et al., 2014). For the global topology parameters of the cortical thickness-based structural covariance network (**Figure 2**), the OCD nonresponders (compared with the OCD responders and HCs) had a significantly shortened *lambda* and a significantly elevated *sigma* ($p < .05$ across the sparsity ranges $0.08 \leq K \leq 0.12$, two-tailed, Kruskal-Wallis one-way analysis of variance). By contrast, no group effect on the *gamma* and *Q* was observed ($p > .05$, two-tailed). Each step of the graph theoretical analysis was conducted using the Brain Connectivity Toolbox (http://www.brain-connectivity-toolbox.net) (Rubinov and Sporns, 2010).

Eigenvector centrality (EC), the mathematical principle behind Google's PageRank algorithm, is a recursive centrality measure that reflects the various layers of hierarchy in a given network (Binnewijzend et al., 2014; Bryan and Leise, 2006l Teicher et al., 2014). We chose the nonrandom sparsity range $0.07 \leq K \leq 0.15$ as a meaningful sparsity range of the cortical thickness-based CMF network to compute the EC, in which range the graphs fulfilled small-worldness (*lambda* ≈ 1, *gamma* > 1, and *sigma* > 1) and modular topology ($Q > 0.3$) with the presence of false-positive edges minimized (**Figure 1(B)**) (He et al., 2008; Uehara et al., 2014). Accordingly, for each group (HCs, OCD responders and nonresponders), the hub nodes (**Table 1**) were selected based on the criterion of the top 12% of ROIs ranked using the z-scored EC values at the group-

averaged CMF network across the sparsity range $0.07 \leq K \leq 0.15$ (He et al., 2008; Teicher et al., 2014; van den Heuvel et al., 2013). The top 18 hub nodes (ROIs) according to the average value of the z-scored EC for each group (HCs, OCD responders and nonresponders) included the bilateral superior circular sulcus of the insula, dorsolateral prefrontal cortex (DLPFC), middle cingulate cortex (MCC), supramarginal gyrus and angular gyrus of the IPL, and middle occipital gyrus. In addition, the OCD responders and nonresponders had overlapping hub nodes that included the right pars triangularis and the bilateral ventral/dorsal ACC (vACC/dACC). The left central operculum served as a hub node for both the OCD responders and HCs, whereas the HCs and OCD nonresponders shared hub nodes in the left superior frontal sulcus, left precuneus and right central operculum (**Table 1**).

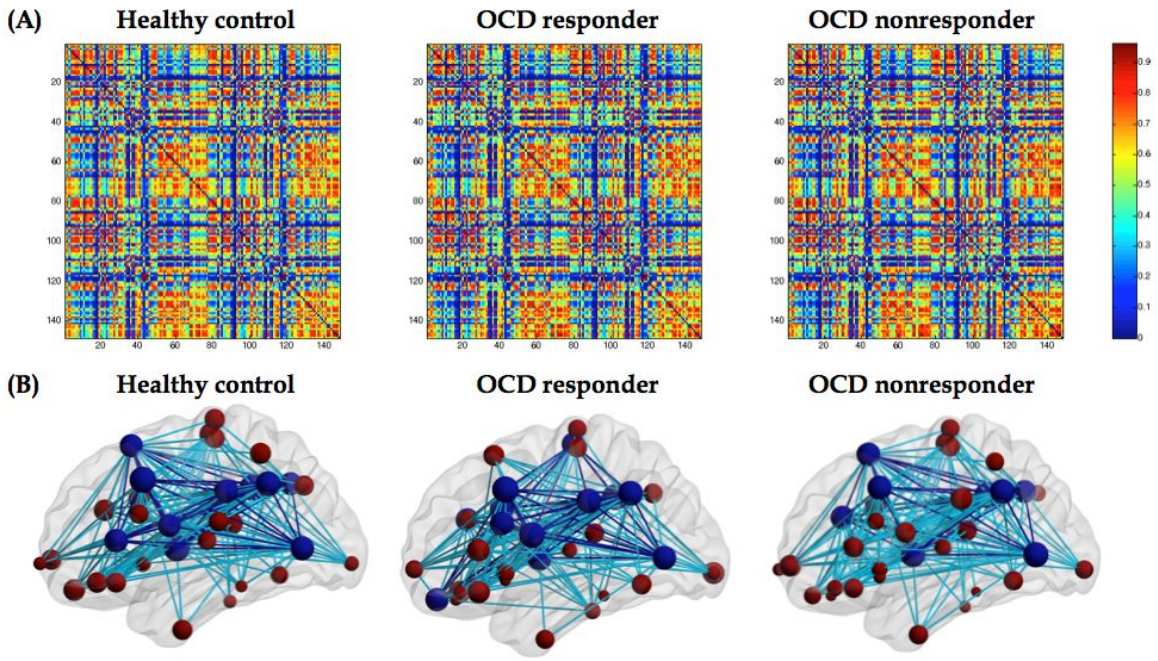

Figure 1. Individualized cortical thickness-based structural covariance networks of healthy controls (left column), obsessive-compulsive disorder (OCD) treatment responders (middle column) and OCD treatment nonresponders (right column). **(A)** Correlative morphological feature matrix (group-averaged; values ranged from 0 to 1 as indicated by the color bar) comprising the structural covariance network. **(B)** Graph theory analysis. Hub-related connections (dark blue lines) between hub nodes (dark blue spheres; top 12% nodes ranked using the *z-scored* eigenvector centrality; refer to Table 2), as well as feeder connections (light blue lines) between the hub nodes and non-hub nodes (brown spheres) in the cortical thickness-based structural covariance network were calculated across the meaningful sparsity range $0.07 \leq K \leq 0.15$, in which the range of the cortical thickness-based structural covariance network fulfilled small-worldness (*lambda* ≈ 1, *gamma* > 1, and *sigma* > 1) and modular topology ($Q > 0.3$) with the false-positive edges minimized. The size of the nodes depicted as spheres represent the *z-scored* eigenvector centrality values group averaged over the sparsity range $0.07 \leq K \leq 0.15$.

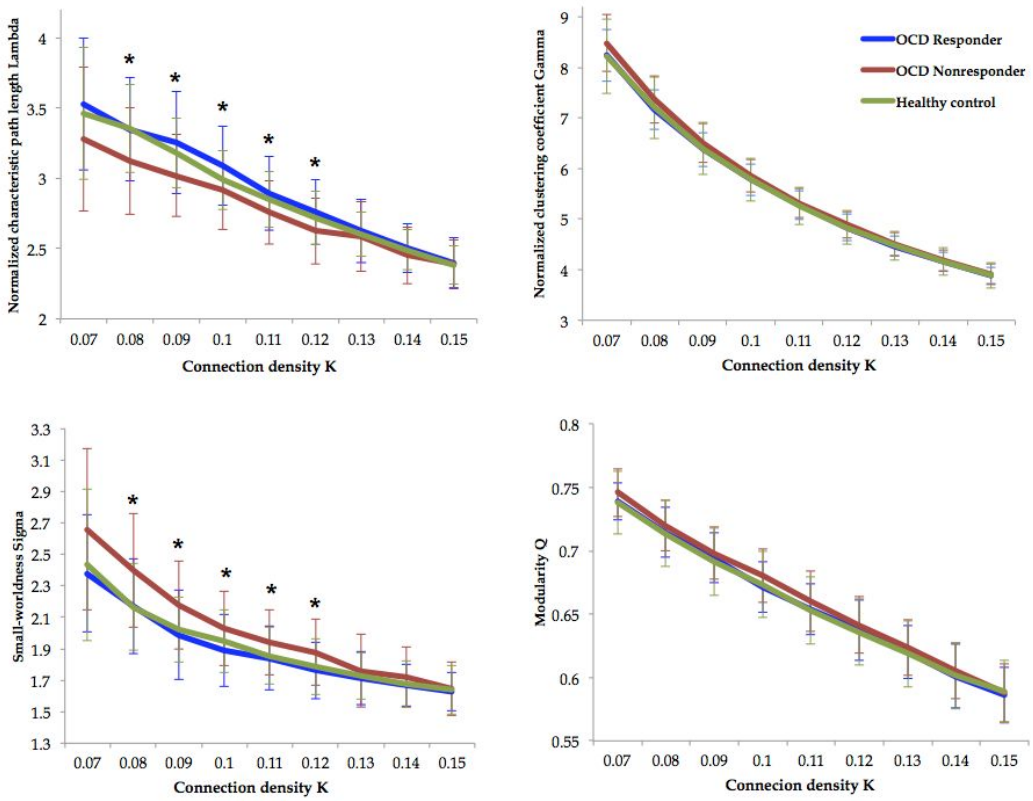

Figure 2. Global parameters (y axis) of the cortical thickness-based structural covariance network in subjects with obsessive-compulsive disorder (OCD) and healthy controls at various sparsity ranges of $0.07 \leq K \leq 0.15$. Solid lines and error bars (blue, OCD responder; red, OCD nonresponder; green, healthy control) represent for the average values and standard deviations of the normalized characteristic path length (*lambda*; upper left), the normalized clustering coefficient (*gamma*; upper right), the small-worldness parameter *sigma* (lower left), and the modularity *Q* (lower right), respectively. *Lambda* and *sigma* (at the sparsity ranges of $0.08 \leq K \leq 0.12$; $P < 0.05$, Kruskal-Wallis one way analysis of variance) were significantly different among the three groups of OCD nonresponders, OCD responders and healthy controls. *$P < 0.05$.

TABLE 1

Hub regions ranked as the top 18 among the whole 148 regions of interest according to their eigenvector centrality values in the group-averaged structural covariance network (over the sparsity ranges of *0.07 ≤ K ≤ 0.15*)

Healthy Controls (N=75)	EC	OCD Responder (N=25)	EC	OCD Nonresponder (N=31)	EC
Right superior circular sulcus of insula	2.026	Left DLPFC	2.018	Left MCC	2.263
Left DLPFC	2.020	Right superior circular sulcus of insula	1.985	Left middle occipital cortex	2.179
Right MCC	2.011	Right MCC	1.964	Left superior circular sulcus of insula	2.029
Left superior circular sulcus of insula	1.929	Left central operculum	1.869	Right DLPFC	2.020
Right supramarginal gyrus of IPL	1.900	Right angular gyrus of IPL	1.864	Left angular gyrus of IPL	2.017
Left MCC	1.852	Right DLPFC	1.819	Right superior circular sulcus of insula	1.993
Right DLPFC	1.817	Left supramarginal gyrus of IPL	1.694	Left DLPFC	1.968
Right angular gyrus of IPL	1.804	Left angular gyrus of IPL	1.672	Right MCC	1.905
Left angular gyrus of IPL	1.655	Right pars triangularis	1.661	Left superior frontal sulcus	1.869
Left middle occipital cortex	1.604	Left superior circular sulcus of insula	1.575	Left vACC	1.819
Right middle occipital cortex	1.601	Right middle occipital cortex	1.574	Right middle occipital cortex	1.739
Left pars triangularis	1.495	Left middle occipital cortex	1.527	Right pars triangularis	1.721
Left supramaginal gyrus of IPL	1.468	Right supramarginal gyrus of IPL	1.505	Right angular gyrus of IPL	1.701
Right primary motor cortex	1.420	Left primary motor cortex	1.485	Left precuneus	1.650
Left superior frontal sulcus	1.417	Left pars opercularis	1.483	Right supramarginal gyrus of IPL	1.646
Left precuneus	1.404	Left dACC	1.474	Right vACC	1.570
Right central operculum	1.404	right vACC	1.474	Right dACC	1.539
Left cetral operculum	1.397	Left OFC	1.446	Right primary motor cortex	1.484

Abbreviations: dACC: dorsal anterior cingulate cortex; DLPFC: dorsolateral prefrontal cortex; EC: normalized eigenvector centrality; IPL: inferior parietal lobule; MCC: middle cingulate cortex; OFC: orbitofrontal cortex; vACC: ventral anterior cingulate cortex.

5. Individualized, Cortical Thickness or Cortical Surface Area-Based Structural Covariance Network

Based on the result of initial graph theory-based investigation for cortical thickness-related CMF, using both cortical surface area and cortical thickness values per subject, we calculated individualized cortical thickness or cortical surface area-based structural covariance network and used selected features of this network for final support vector machine experiments as group classifier. Firstly, we regressed-out inter-individual cerebral hemispheric size differences from cortical morphological values of mean CSA or mean CT for ROI *i* [*i* = 1-148] per subject *k*, using the total CSA value or mean and standard deviation values of CT per each individual, respectively (Kremen et al., 2013).

$$CSA_k(i) = (CSA_k(i) / CSA\_total_k)$$
$$CT_k(i) = \left[(CT_k(i) - CT\_mean_k) / CT\_sd_k \right]$$

Thereafter, we calculated the CSA-ISC or CT-ISC value, of ROI(*i)* vs. ROI(*j)* for subject *k* ($CSA\_ISC_k(i,j)$ or $CT\_ISC_k(i,j)$, respectively; subject *k* could be either OCD or HC) using the following formula [Wee et al., 2013]:

$$CSA\_ISC_k(i,j) = 1 / \exp\left(\left(CSA\_zscored_k(i) - CSA\_zscored_k(j) \right)^2 \right)$$
$$CT\_ISC_k(i,j) = 1 / \exp\left(\left(CT\_zscored_k(i) - CT\_zscored_k(j) \right)^2 \right)$$

where $CSA\_zscored_k(i)$ and $CT\_zscored_k(i)$ were computed as

$$CSA\_zscored_k(i) = (CSA_k(i) - CSA_M(i)) / CSA_{SD}(i)$$
$$CT\_zscored_k(i) = (CT_k(i) - CT_M(i)) / CT_{SD}(i)$$

$CSA_M(i)$ and $CSA_{SD}(i)$ denote the regional mean and standard deviation of CSA in *ROI(i)* across all HCs (*n* = 75). These formulae were converted into a Matlab script as

demonstrated below;

```
% (These cortical morphologic variables used in this script ['bert'] were
% implemented in the '/subjects/bert' directory of FreeSurfer software ver
% 5.3.0.);


% Calculate csa_k and ct_k

bert_csa_total(1,1)=sum(bertcsalh{1,2:75})+sum(bertcsarh{1,2:75});
for j=1:74
    bert_csa_norm(j,1)=bertcsalh{1,j+1}./bert_csa_total(1,1);
end
for j=75:148
    bert_csa_norm(j,1)=bertcsarh{1,j-73}./bert_csa_total(1,1);
end

bert_ct_concat=[bertctlh{1,2:75},bertctrh{1,2:75}];
bert_mean_ct(1,1)=mean(bert_ct_concat,2);
bert_sd_ct(1,1)=std2(bert_ct_concat);
for j=1:74
    bert_ct_norm(j,1)=(bertctlh{1,j+1}-bert_mean_ct)./bert_sd_ct;
end
for j=75:148
    bert_ct_norm(j,1)=(bertctrh{1,j-73}-bert_mean_ct)./bert_sd_ct;
end


% Calculate csa_zscored and ct_zscored using csa_k and ct_k, respectively
% CSA_BASE_HC_NORMALIZED_ROI_MEAN & CSA_BASE_HC_NORMALIZED_ROI_SD as well as
% CT_BASE_HC_NORMALIZED_ROI_MEAN & CT_BASE_HC_NORMALIZED_ROI_SD were
% pre-calculated [with exactly same manner as desribed above for 'bert']
% using the given values of healthy controls(n=75) participated in this study

for i=1:148
    bert_csa_zscored(i,1)=(bert_csa_norm(i,1)- ...
CSA_BASE_HC_NORMALIZED_ROI_MEAN(i,1))./CSA_BASE_HC_NORMALIZED_ROI_SD(i,1);
    bert_ct_zscored(i,1)=(bert_ct_norm(i,1)- ...
CT_BASE_HC_NORMALIZED_ROI_MEAN(i,1))./CT_BASE_HC_NORMALIZED_ROI_SD(i,1);
end


% Calculate CSA-ISC and CT-ISC per subject

CSA_ISC_bert=zeros(148,148);
CT_ISC_bert=zeros(148,148);
```

```
for k=1:148
    for t=1:148
        CSA_ISC_bert(k,t)=1./exp((bert_csa_zscored(k,1)- ...
bert_csa_zscored(t,1))^2);
        CT_ISC_bert(k,t)=1./exp((bert_ct_zscored(k,1)-bert_ct_zscored(t,1))^2);
    end
end

for p=1:148
    CSA_ISC_bert(p,p)=0;
    CT_ISC_bert(p,p)=0;
end


% visualize final CSA-ISC and CT-ISC

figure

subplot(1,2,1)
imagesc(CSA_ISC_bert)
hold on
colorbar
hold on
title('CSA-ISC for Bert')
hold off

subplot(1,2,2)
imagesc(CT_ISC_bert)
hold on
colorbar
hold on
title('CT-ISC for Bert')
hold off
```

After calculation of the CSA-ISC or CT-ISC values between the 148 numbers of ROIs for each subject, only the most informative ISCs showing statistical significance (uncorrected $p < .001$ [two-tailed], independent t-tests) across every n runs of leave-one-out group-comparison (n = 56 for OCD-R vs. OCD-NR; n = 100 for OCD-R vs. HC; n = 106 for OCD-NR vs. HC) [Dosenbach et al., 2010] were aligned according to the absolute value of averaged t-statistics and were packaged into candidate feature sets

(*S_CSA_group-A_group-B(k/n) or S_CT_group-A_group-B(k/n), 1 ≤ k ≤ n, n* = maximum number of candidate feature) for classification analysis using SVM method.

6. Support Vector Machine

The most informative ISCs (uncorrected $p < .001$ [two-tailed], independent t-tests) across every *n* runs of leave-one-out group-comparison ($n = 56$ for OCD-R vs. OCD-NR; $n = 100$ for OCD-R vs. HC; $n = 106$ for OCD-NR vs. HC) (Dosenbach et al., 2010) packaged into candidate feature sets were used as group classifier in final SVM-based (non-linear radial basis function kernel [*sigma = 2*]; constant soft-margin [*cost = 1*]) group classification analyses using Statistics Toolbox of the Matlab software package (ver. R2014b; MathWorks Inc., Natick, MA, USA).

All SVM training, testing and iterative group separation of subjects into training and procedures permutation using random for cross-validation were repeated 10,000 times per candidate feature set. In the SVM training procedure to distinguish OCD-R from OCD-NR, using a training dataset of 46 subjects randomly collected from the 56 total OCDs, the decision boundary formulated using a candidate feature set was optimized to maximize group classification accuracy.

During the testing phase, a test dataset of 10 OCDs, not disclosed in the SVM training phase, was classified as OCD-R or OCD-NR using the decision solution for a given observation *x* ($1 \le x \le 10$) based on a given candidate feature set (Dosenbach et al., 2010). In case of distinguishing HCs from OCD-R or OCD-NR subjects separately,

random pre-selection of HCs (n = 25 for OC-R vs. HC, n = 31 for OCD-NR vs. HC) preceded the division of subjects into 40 (for OCD-R vs. HC) or 52 (for OCD-NR vs. HC) training subjects and 10 testing subjects (van Waarde et al., 2014) preceded every cycle of SVM model training and testing. Finally, the most accurate group classifier, evidenced by its highest overall mean accuracy across the 10,000 cross-validation procedures (p < .001, two-tailed and Bonferroni-corrected; independent t-test), was referred to as 'neuroanatomical decision functions of SVM' (**Figure 3-5** and **Table 3-5**).

III. RESULTS

1. Demographic and Clinical Characteristics

The demographic and clinical characteristics of the subjects are summarized in **Table 2**. There were no statistically significant differences among the HCs, OCD responders and OCD nonresponders in terms of age (all OCD subjects versus HCs), sex, and years of education (all $p > .05$; two-tailed). After 4 months of pharmacotherapy, the OCD subjects were divided into two subgroups, responders ($N = 25$; change in the Y-BOCS total score $\geq 35.5\%$) and nonresponders ($N = 31$; change in the Y-BOCS total score $\leq 30\%$).

During the 4-month period of SRI-based pharmacotherapy, the SRI prescribed most often was escitalopram (responders, $N = 25$, average dose per subject = 20.39 mg/day, mean maximum dose per subject = 31.00 mg/day; nonresponders, $N = 27$, average dose per subject = 19.41 mg/day, mean maximum dose per subject=32.25 mg/day). No significant differences were found in the average dosage (t = -0.241, df = 49.05, p = 0.811) or the mean maximum dose ($t = -0.265$, $df = 46.57$, $p = .792$) of escitalopram prescribed per subject between the OCD responders and nonresponders. A total of 8 subjects were prescribed fluoxetine (responders, $N = 2$, average dose prescribed = 24.33 mg/day; nonresponders, $N = 6$, average dose prescribed = 34.75 mg/day), because they had been previously prescribed escitalopram and it was either ineffective ($N = 6$) or caused side effects ($N = 2$; each for nausea and for dizziness), which prevented its continued use. One responder and four nonresponders were given a serotonin-dopamine antagonist to boost the clinical efficacy of the SRI treatment.

Table 2

Demographic and Clinical Characteristics of the Subjects with Obsessive-Compulsive Disorder and the Healthy Control Subjects

Characteristics	OCD responders (*N*=25)	OCD nonresponders (*N*=31)	Healthy controls (*N*=75)	χ^2/T/F	d.f.	*P*
Demographics						
Sex, No. (%)[a]						
Male	16 (64)	19 (61.29)	46 (61.33)	0.06	2.00	.86
Female	9 (36)	12 (38.71)	29 (38.67)			
Age, mean (SD), years[b]	23.45 (5.42)	27.19 (5.94)	25.11 (5.46)	3.17	2.00	.05
Education level, mean (SD), years[b]	13.88 (1.81)	14.61 (2.22)	14.47 (1.72)	1.22	2.00	.30
Age of onset, mean (SD), years[b]	17.24 (6.77)	17.84 (5.75)	-	-0.35	47.3	.73
Duration of illness, mean (SD), years[b]	6.77 (5.77)	9.56 (7.35)	-	-1.16	54.00	.12
Y-BOCS[c]						
Baseline, mean (SD)	27.20 (5.04)	28.19 (5.56)	-	-0.70	53.21	.49
Follow-up, mean (SD)	12.75 (4.23)	24.42 (5.71)	-	-8.70	52.92	< .001
HAM-D[c]						
Baseline, mean (SD)	9.56 (5.37)	11.03 (5.97)	-	-0.97	53.31	.34
Follow-up, mean (SD)	2.88 (3.00)	8.13 (4.64)	-	-5.08	51.53	< .001
HAM-A[c]						
Baseline	8.32 (4.44)	11.35 (6.51)	-	-2.07	52.68	.04
Follow-up	5.21 (3.83)	5.19 (4.06)	-	0.01	50.88	.99

Abbreviations: d.f., degree of freedom; HAM-A, Hamilton Anxiety Rating Scale; HAM-D, Hamilton Rating Scale for Depression; OCD, obsessive-

compulsive disorder; Y-BOCS, Yale-Brown Obsessive Compulsive Scale.

[a]Differences between the variables in the three groups were assessed using the chi-square test.

[b]Differences between the variables in the three groups were assessed using analysis of variance.

[c]Differences between the variables in the two groups were assessed using an independent t-test.

2. Multivariate Pattern Classification Analysis: OCD-R vs. OCD-NR

The optimum group classifier, *i.e.,* the 'neuroanatomical decision function,' used to classify OCD-R from OCD-NR (**Figure 3** and **Table 4**), which encompassed a feature set of the top 12 ISCs ranked according to the size of averaged t-statistics, demonstrated the most accurate classification performance with an overall accuracy of 89.0% (**Table 3**). Of note, a CT-ISC between the right superior frontal sulcus (superior border of dorsolateral prefrontal cortex [DLPFC]) and left marginal branch of the cingulate sulcus (anterior border of precuneus) served as components of the neuroanatomical decision function in distinguishing the OCD-R from both the HCs and the OCD-NR. Also, a CSA-ISC between the left short insular gyrus (anterior part of insula [AI]) versus left intraparietal sulcus (IPS) served as a key component of the neuroanatomical decision function in distinguishing OCD-NR from both HCs and OCD-R. Moreover, two intra-network CSA/CT-ISCs of the bilateral perisylvian language network-related regions including inferior frontal, superior and middle temporal cortices (Leroy et al., 2011) as well as five inter-network CSA/CT-ISCs with bilateral precuneus and visual association cortices were used as components of an optimal feature set which successfully classified OCD-R from OCD-NR.

Table 3

Averaged Group Classification Performance of the Most Accurate Group Classifier Called 'neuroanatomical decision functions': Performance of the Support Vector Machine (SVM) training, Testing as well as the Iterative Group Separation with Random Permutation of Subjects into Training (n = 56 for OCD-responder vs. OCD-nonresponder; n = 100 for OCD-responder vs. HC; n = 106 for OCD-nonresponder vs. HC) and Testing sets (n = 10) for Cross-Validation were Repeated for 10,000 Times.

Binary classifier	R vs. NR[b]	R vs. HC[c]	NR vs HC[d]
Cortical Surface Area- or Thickness-Based, Individualized Structural Covariance			
True positive, mean (SD)	3.9 (1.4)	4.7 (1.4)	4.6 (1.4)
True negative, mean (SD)	5.0 (1.4)	4.8 (1.4)	4.5 (1.4)
False positive, mean (SD)	0.5 (0.7)	0.2 (0.4)	0.5 (0.7)
False negative, mean (SD)	0.6 (0.7)	0.3 (0.5)	0.5 (0.7)
Sensitivity, mean (SD) (%)	88.4 (15.7)	96.2 (8.9)	90.8 (13.3)
Specificity, mean (SD) (%)	90.1 (12.4)	95.0 (9.7)	91.1 (13.4)
Accuracy, mean (SD) (%)	89.0 (8.9)	95.6 (6.1)	90.7 (8.8)
Positive predictive value, mean (SD) (%)	88.0 (15.0)	95.2 (9.4)	91.4 (12.8)
Negative predictive value, mean (SD) (%)	90.7 (12.6)	96.5 (8.3)	90.9 (13.1)

Abbreviations: HC, healthy control; NR, treatment nonresponder subjects with obsessive-compulsive disorder; R, treatment responder subjects with obsessive-compulsive disorder.

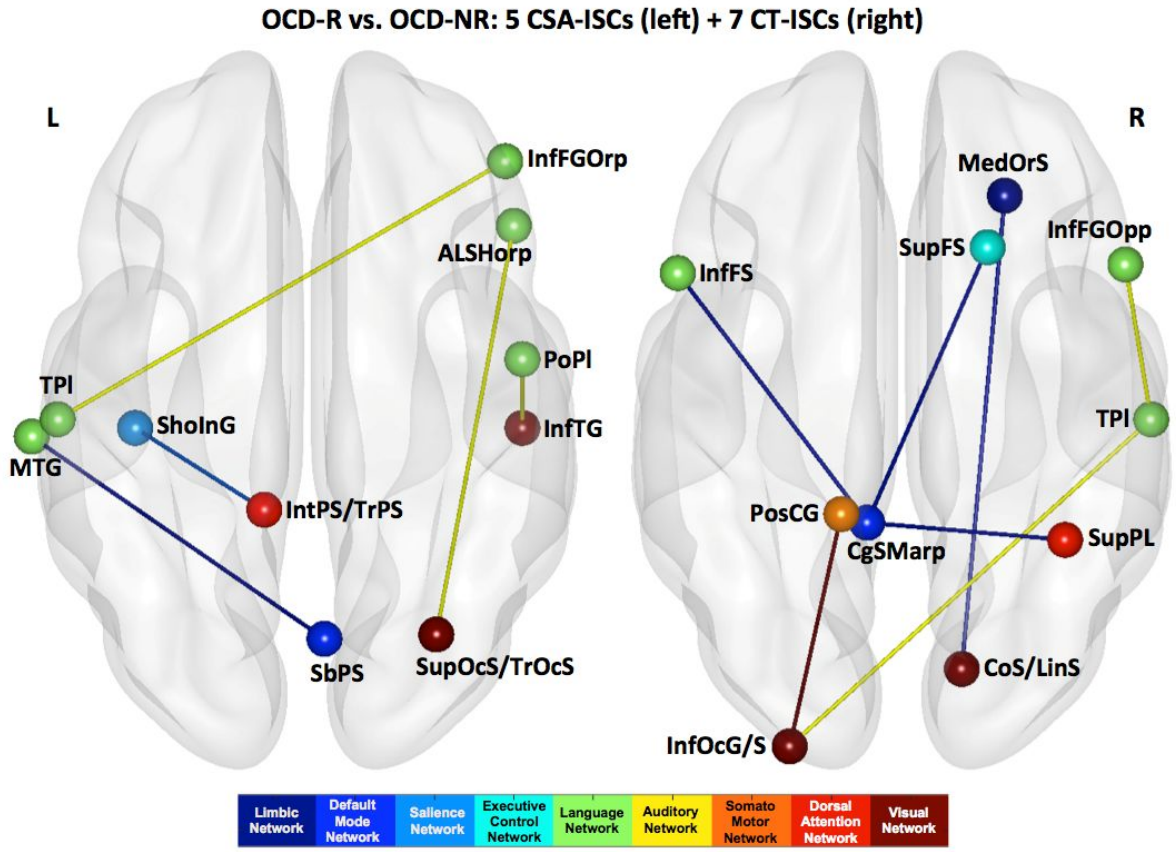

Figure 3. The optimal neuroanatomical decision function comprised of five cortical surface area-based individualized structural covariance (CSA-ISC) as well as seven cortical thickness-based individualized structural covariance (CT-ISC) features successfully (mean accuracy of 89.0%) classified subjects with obsessive-compulsive disorder (OCD) into responders or nonresponders for serotonin reuptake inhibitor-based pharmacotherapy.

Abbreviations: ALSHorp, horizontal ramus of the anterior segment of the lateral sulcus; CgSMarp, marginal branch of the cingulate sulcus; CoS/LinS, medial occipito-temporal sulcus and lingual sulcus; InfFGOpp, pars opercularis; InfFGOrp, pars orbitalis; InfFS, inferior frontal sulcus; InfOcG/S, inferior occipital gyrus and sulcus; InfTG, inferior temporal gyrus; IntPS/TrPS, intraparietal sulcus; L, left; MedOrS, medial orbital sulcus; MTG, middle temporal gyrus; PoPI, planum polare; PosCG, postcentral gyrus; R, right; SbPS, subparietal sulcus;

ShoInG, short insular gyri; SupFS, superior frontal sulcus; SupOcS/TrOcS, superior and transverse occipital sulci; SupPL, superior parietal lobule; TPl, planum temporale.

Table 4

Neuroanatomical Decision Functions of Support Vector Machine Model: Classification of Subjects with Obsessive-Compulsive Disorder into Responders or Nonresponders for Serotonin Reuptake Inhibitor-Based Pharmacotherapy

Rank	CLASS	ROI_I	ROI_J	ROI_I_name	ROI_J_name	LOOGC_T
1	CT	36	76	Rt. planum temporale	Lt. inferior occipital gyrus/sulcus	-4.330
2	CSA	39	58	Rt. horizontal ramus of the anterior segment of the lateral sulcus	Rt. transverse occipital sulcus	-4.316
3	CSA	71	112	Rt. subparietal sulcus	Lt. middle temporal gyrus	-4.204
4	CT	27	82	Rt. superior parietal lobule	Lt. middle-posterior cingulate gyrus/sulcus	-4.029
5	CSA	92	130	Lt. short insular gyrus	Lt. intraparietal sulcus	-3.970
6	CSA	35	37	Rt. planum polare	Rt. inferior temporal gyrus	3.928
7	CT	120	126	Lt. marginal branch of the cingulate sulcus	Lt. inferior frontal sulcus	-3.888
8	CSA	13	110	Rt. pars orbitalis	Lt. planum temporale	-3.852
9	CT	54	120	Rt. superior frontal sulcus	Lt. marginal branch of the cingulate sulcus	-3.793
10	CT	76	102	Lf. inferior occipital gyrus/sulcus	Lt. postcentral gyrus	-3.777
11	CT	61	63	Rt. collateral sulcus	Rt. medial orbital sulcus	3.750
12	CT	12	36	Rt. pars opercularis	Rt. planum temporale	-3.743

Abbreviations: CSA, cortical surface area; CT, cortical thickness; LOOGC_T, averaged value of T statistics over the whole leave-one-out group-comparison; Lt=left; ROI=region of interest; Rt=right.

3. Multivariate Pattern Classification Analysis: OCD-R or vs. HC

An optimal feature set comprising 19 ISCs (**Table 5** and **Figure 4**) distinguished OCD-R from HC subjects with a mean accuracy of 95.6% (sensitivity = 96.2%; specificity = 95.0%; **Table 3**). Ten CSA-ISCs, bilateral anterior segment of the circular sulci of the insula and left supramarginal gyrus as well as bilateral planum temporale and central operculum showed altered strength of CSA-ISCs with other posterior brain regions in OCD-R compared to HC. In addition, nine CT-ISCs between the left posterior cingulate gyrus (PCC), bilateral angular gyri and right superior temporal sulcus versus other superior frontal and parieto-occipital brain regions were also successfully contributed in classification of OCD-R from HC using the SVM.

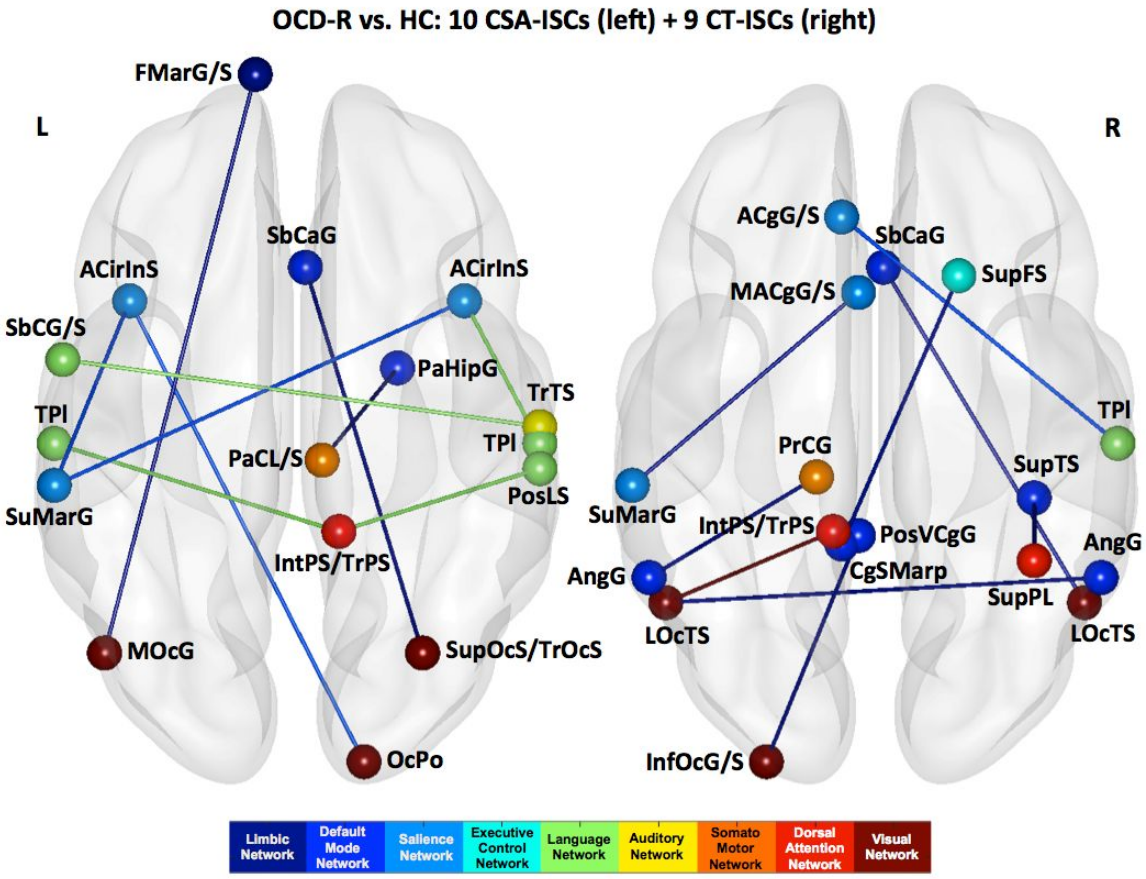

Figure 4. The optimal neuroanatomical decision function comprised of 10 cortical surface area-based individualized structural covariance (CSA-ISC) as well as nine cortical thickness-based individualized structural covariance (CT-ISC) features successfully (mean accuracy of 95.6%) classified pharmacotherapy-responsive subjects with obsessive-compulsive disorder from Healthy Controls.

Abbreviations: ACgG/S, anterior cingulate gyrus and sulcus; ACirInS, anterior segment of the circular sulcus of the insula; AngG, angular gyrus; CgSMarp, marginal branch of the cingulate sulcus; FMarG/S, fronto-marginal gyfigure rus and sulcus; InfOcG/S, inferior occipital gyrus and sulcus; IntPS/TrPS, intraparietal and transparietal sulci; L, left; LOcTS, lateral occipito-temporal sulcus; MACgG/S, middle-anterior part of the cingulate gyrus and sulcus; MOcG, middle occipital gyrus; OCPo, occipital pole; PaCL/S, paracentral lobule and sulcus; PaHipG, parahippocampal gyrus; PosLS, posterior ramus of the lateral sulcus; PosVCgG, posterior-

ventral part of the cingulate gyrus; PrCG, precentral gyrus; R, right; SbCaG, subcallosal gyrus; SbCG/S, subcentral gyrus and sulci; SuMarG, supramarginal gyrus; SupFS, superior frontal sulcus; SupOcS/TrOcS, superior and transverse occipital sulci; SupPL, superior parietal lobule; SupTS, superior temporal sulcus; TPl, planum temporale; TrTS, transverse temporal sulcus.

Table 5. Neuroanatomical Decision Functions of Support Vector Machine Model: Classification of Subjects with Obsessive-Compulsive Disorder Responders from Healthy Controls

Rank	CLASS	ROI_I	ROI_J	ROI_I_name	ROI_J_name	LOOGC_T
1	CSA	74	78	Rt. transverse temporal sulcus	Lt. central operculum/sulci	4.819
2	CSA	36	47	Rt. planum temporale	Rt. anterior segment of the circular sulcus of the insula	-4.768
3	CSA	42	121	Rt. occipital pole	Lt. anterior segment of the circular sulcus of the insula	-4.765
4	CSA	3	23	Rt. paracentral gyrus/sulcus	Rt. parahippocampal gyrus	4.535
5	CT	25	134	Rt. angular gyrus	Lt. lateral occipito-temporal sulcus	4.478
6	CSA	100	121	Lt. supramarginal gyrus	Lt. anterior segment of the circular sulcus of the insula	-4.376
7	CSA	32	58	Rt. subcallosal gyrus	Rt. superior/transverse occipital sulcus	-4.088
8	CT	99	103	Lt. angular gyrus	Lt. precentral gyrus	4.038
9	CT	81	100	Lt. aMCC	Lt. supramarginal gyrus	4.018
10	CT	54	120	Rt. superior frontal sulcus	Lt. marginal branch of the cingulate sulcus	-3.998
11	CT	32	60	Rt. subcallosal gyrus	Rt. lateral occipito-temporal sulcus	-3.986
12	CT	27	73	Rt. superior parietal lobule	Rt. superior temporal sulcus	-3.911
13	CSA	47	100	Rt. anterior segment of the circular sulcus of the insula	Lt. supramarginal gyrus	-3.880
14	CSA	41	56	Rt. posterior ramus of the lateral sulcus	Rt. intraparietal sulcus	-3.827
15	CT	130	134	Lt. intraparietal sulcus	Lt. lateral occipito-temporal sulcus	3.799
16	CSA	75	93	Lt. frontomarginal gyrus/sulcus	Lt. middle occipital gyrus	-3.792
17	CT	36	80	Rt. planum temporale	Lt. dACC	-3.784
18	CSA	56	110	Rt. intraparietal sulcus	Lt. planum temporale	-3.768
19	CT	76	84	Lt. inferior occipital gyrus/sulcus	Lt. vPCC	-3.721

Abbreviations: CSA, cortical surface area; CT, cortical thickness; dACC, dorsal anterior cingulate cortex; LOOGC_T, averaged value of T statistics over the whole leave-one-out group-comparison; Lt=left; MCC, middle cingulate cortex; PCC, posterior cingulate cortex; ROI=region of interest; Rt=right.

4. Multivariate Pattern Classification Analysis: OCD-NR or vs. HC

On the other hand, an optimal feature set of neuroanatomical decision function comprising 16 CSA-ISC or CT-ISCs (**Table 6** and **Figure 5**) could classify OCD-NR from HC subjects with a mean accuracy of 90.7% (sensitivity = 90.8%; specificity = 91.1%; **Table 3**). Eight CSA-ISCs in the right OFC and pars orbitalis, planum polare and left planum temporale as well as right PCC with posterior brain regions could successfully classify the OCD-NR from HC. Moreover, eight CT-ISCs in the left inferior frontal sulcus and lateral superior temporal gyrus as well as in the right anterior horizontal ramus of the lateral sulcus and middle temporal gyrus with other fronto-parietal regions were also participated in accurate classification of OCD-NR from HC.

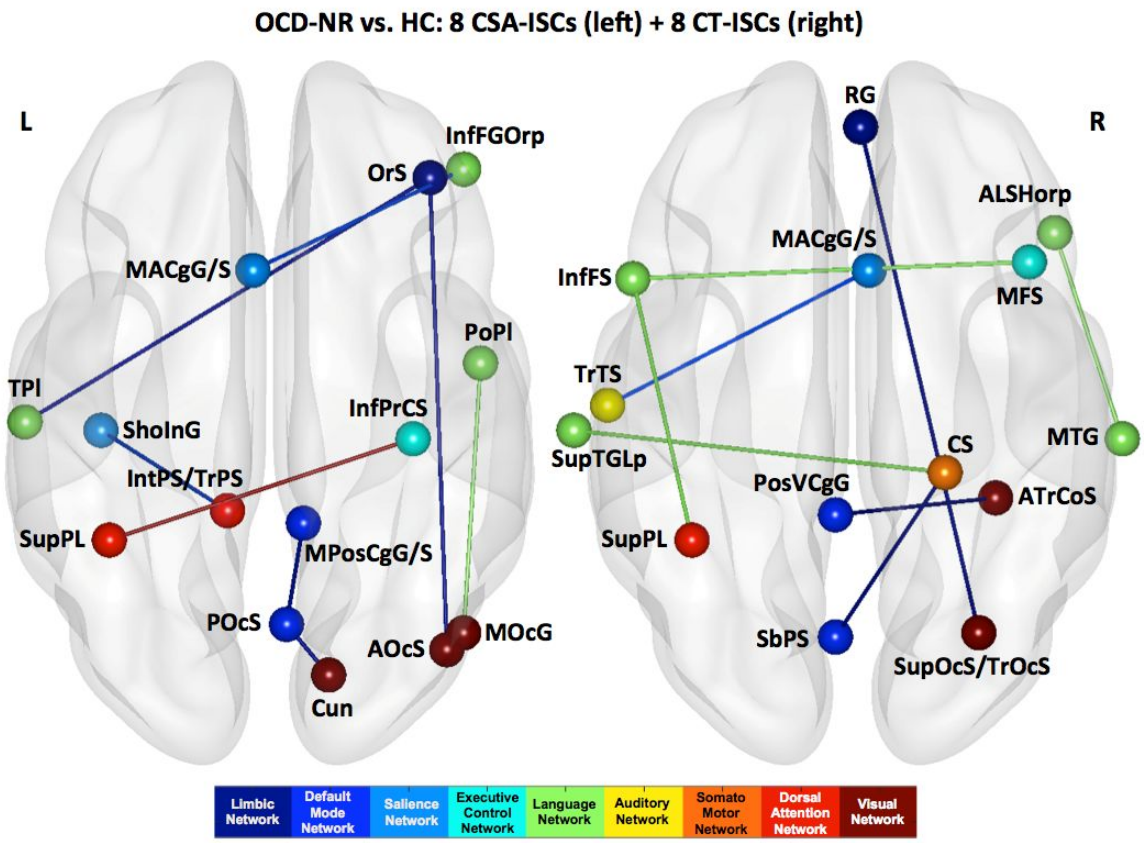

Figure 5. The optimal neuroanatomical decision function comprised of eight cortical surface area-based individualized structural covariance (CSA-ISC) as well as eight cortical thickness-based individualized structural covariance (CT-ISC) features successfully (mean accuracy of 90.7%) classified pharmacotherapy-nonresponsive subjects with obsessive-compulsive disorder from Healthy Controls.

Abbreviations: ALSHorp, horizontal ramus of the anterior segment of the lateral sulcus; AOcS, anterior occipital sulcus and preoccipital notch; ATrCoS, anterior transverse collateral sulcus; CS, central sulcus; Cun, cuneus; InfFGOrp, pars orbitalis; InfFS, inferior frontal sulcus; InfPrCS, inferior part of the precentral sulcus; IntPS/TrPS, intraparietal and transparietal sulci; L, left; MACgG/S, middle-anterior part of the cingulate gyrus and sulcus; MFS, middle frontal sulcus; MOcG, middle occipital gyrus; MPosCgG/S, middle-posterior part of the cingulate gyrus and sulcus; MTG, middle temporal gyrus; OrS, orbital sulci (H-shaped); POcS, parieto-occipital sulcus; PoPl, planum polare; PosVCgG, posterior-ventral part of the cingulate gyrus; R, right;

RG, gyrus rectus; SbPS, subparietal sulcus; ShoInG, short insular gyri; SupOcS/TrOcS, superior and transvers occipital sulci; SupPL, superior parietal lobule; SupTGLp, lateral aspect of the superior temporal gyrus; TPl, planum temporale; TrTS, transverse temporal sulcus.

Table 6

Neuroanatomical Decision Functions of Support Vector Machine Model: Classification of Subjects with Obsessive-Compulsive Disorder Nonresponders from Healthy Controls

rank	CLASS	ROI_I	ROI_J	ROI_I_name	ROI_J_name	LOOGC_T
1	CT	31	58	Rt. gyrus rectus	Rt. superior/transverse occipital sulcus	-4.481
2	CSA	92	130	Lt. short insular gyrus	Lt. intraparietal sulcus	4.427
3	CSA	59	64	Rt. anterior occipital sulcus	Rt. orbital sulci (H-shaped)	-4.425
4	CT	45	145	Rt. central sulcus	Lt. subparietal sulcus	-4.349
5	CT	101	126	Lt. superior parietal lobule	Lt. inferior frontal sulcus	4.301
6	CT	50	84	Rt. anterior transverse collateral sulcus	Lt. vPCC	-4.261
7	CT	45	108	Rt. central sulcus	Lt. lateral aspect of the superior temporal gyrus	-4.144
8	CT	53	126	Rt. middle frontal sulcus	Lt. inferior frontal sulcus	3.890
9	CT	7	148	Rt. aMCC	Lt. transverse temporal sulcus	3.887
10	CSA	64	110	Rt. orbital sulci (H-shaped)	Lt. planum temporale	-3.709
11	CSA	19	35	Rt. middle occipital gyrus	Rt. planum polare	-3.696
12	CT	38	39	Rt. middle temporal gyrus	Rt. horizontal ramus of the anterior segment of the lateral sulcus	-3.690
13	CSA	68	101	Rt. inferior part of the precentral sulcus	Lt. superior parietal lobule	-3.658
14	CSA	13	81	Rt. pars orbitalis	Lt. aMCC	3.637
15	CSA	8	65	Rt. pMCC	Rt. parieto-occipital sulcus	-3.621
16	CSA	11	65	Rt. cuneus	Rt. parieto-occipital sulcus	-3.620

Abbreviations: CSA, cortical surface area; CT, cortical thickness; LOOGC_T, averaged value of T statistics over the whole leave-one-out group-

comparison; Lt=left; MCC, middle cingulate cortex; ROI, region of interest; ROI=region of interest; Rt=right.

IV. DISCUSSION

1. Key Findings

To the best of our knowledge, this is the first study to elucidate the neural correlates of the treatment response of OCD to SRI-based pharmacotherapy with a SVM classification model, using an individualized cortical morphology-based structural covariance network. Our individualized cortical morphology-based structural covariance satisfied small-world regime [as demonstrated by small-worldness *sigma*] and also met standard of scale-free network [as shown by presence of eigenvector centrality-based hub regions]. After 4 months of SRI-based pharmacotherapy, the subjects with OCD could be divided into two separated subgroups of treatment responders and nonresponders. Indeed, the SVM model constructed using the selected facets of the ISCs retaining robust group difference as demonstrated by leave-one-out group-comparison, including the changed strength of CSA-ISCs and CT-ISCs encompassing the executive control (ECN) (Seeley et al., 2007) and default-mode network (DMN) (Andrews-Hanna et al., 2010), salience (SN) (Seeley et al., 2007) and dorsal attention network (DAN) (Anderson et al., 2010), as well as language or visual network (Jouen et al., 2015), not only predicted the initial prognosis of the subjects with OCD as responders or nonresponders with an accuracy of 89.0% (sensitivity 88.4%, specificity 90.1%) but also distinguished the OCD subjects from the HCs with a 90.7-95.6% accuracy (sensitivity 90.8-96.2%, specificity 91.1-95.0%).

2. An Essential Feature of OCD-R:

Attenuated CT-ISC Between DLPFC [ECN] vs. Precuneus [DMN]

For successful classification of OCD-R from both the HCs and the OCD-NR, a CT-ISC between the right DLPFC (a hub region of ECN) and left precuneus (a hub region of DMN) served as a primal component of the neuroanatomical decision function in this study. Dynamic interaction between DMN and ECN orchestrates self-referential mental simulation with executive control (Liang et al., 2015, Smith et al., 2015). Therefore, attenuated CT-ISC between the DLPFC and precuneus in OCD-R could be related to the inflexible cognitive adaptation for changing environment as well as impaired working memory and emotional regulation in OCD (Shin and Kim, 2015, Van Snellenberg et al., 2015). However, as SRI-based pharmacotherapy could change not only the grey matter volume and baseline glucose metabolism of DLPFC/precuneus but also the DLPFC/precuneus-centered functional connectivity network (Shen et al., 2015, Shin et al., 2014, Wang et al., 2014), this primal feature of OCD-R could also be a biomarker of better treatment response for SRI-based pharmacotherapy in OCD.

3. A Principal Feature of OCD-NR:

Exaggerated CSA-ISC Between AI [SN] vs. IPS [DAN]

In distinguishing OCD-NR from both HCs and OCD-R, a CSA-ISC between the left AI versus left IPS served as a key component of neuroanatomical decision function. Exaggerated CSA-ISC between the left AI versus left IPS in OCD-NR could underlie the imbalance of inter-network crosstalk between SN and DAN and might be result in

salience misattribution and subsequent faulty focusing of attention against the global context of stimuli in OCD (Leaver et al., 2015, Uddin, 2015, Zhang et al., 2015). While noteworthy changes of glucose metabolism or functional activation patterns in AI/IPS as well as regional homogeneity (ReHo; a measure of the synchronization between time-series of a given voxel with its nearest neighboring voxels) (Zang et al., 2004) of insula were detected after SRI-based pharmacotherapy in subjects with depressive or anxiety disorders (Bruhl et al., 2010, Gyurak et al., 2015, Wang et al., 2014), few studies have reported significant changes of AI/IPS-related functional connectivity network after SRI-based pharmacotherapy to date.

4. Differential Strength of Language Network-related CSA/CT-ISCs & Treatment Response in OCD

As components of optimal neuroanatomical decision function, exaggerated strength of language network-related CSA-ISCs or CT-ISCs in OCD-NR compared to OCD-R, not only in the two intra-network ISCs of bilateral perisylvian language network but also in the four inter-network ISCs between the language network versus DMN/visual network, could successfully classify OCD-R from OCD-NR. The comprehensive notion of 'meaning network', supporting effective comprehension of daily events, requires collaboration of semantic processing (language network), spatial perspective taking (visual network) and mentalizing (DMN) (Jouen et al., 2015), all of which components covered with our optimal neuroanatomic decision function (**Figure 3**). Of interest, previous studies for changes of functional activation in inferior frontal or middle temporal regions across the SRI-based pharmacotherapy showed differential treatment

effect in relevance to the task presented; without noticeable improvement of functional activity during verbal fluency task (Tomioka et al., 2015), distinctively changed patterns were detected during the processing of affective (pictures, faces or words) stimuli (Henry et al., 2013, Robertson et al., 2007).

5. Limitations

Because our study aimed to elucidate the clinical value of the cortical structural covariance network (Alexander-Bloch et al., 2013a, Wee et al., 2013), we did not include regional brain morphology statistics on the subcortical structures such as striatum and thalamus (Shaw et al., 2014) as potential components of the neuroanatomical decision function in our SVM classification model. In addition, the further investigation of longitudinal changes in the cortical morphology-based structural covariance network in response to SRI-based pharmacotherapy should be another focus of clinical research (Han et al., 2011, Shin et al., 2014, Yoo et al., 2007).

Moreover, challenging our SVM prediction model using another independent samples (Soriano-Mas et al., 2007) with diverse distribution of demographic [such as age] as well as clinical features [such as degree of comorbid anxiety; our sample revealed differential level of comorbid anxiety at baseline (p = 0.04)] could strengthen the generalizability of our neuroanatomical decision function constructed using the CSA-ISC and CT-ISC. Considering the relatively simple requirement of our predictive SVM model for the new testing data, which were not a raw MRI data per se (which retains the restriction of compatibility of the MRI parameters between the training and

testing data), but rather a set of CMFs calculated from the cortical morphological measurements, our SVM prediction model could be further utilized in the diverse outpatient clinics with their own MRI data.

V. CONCLUSIONS

Our search for biomarkers that predict the clinical treatment response to SRI-based pharmacotherapy in patients with OCD has initiated an investigation of the dysfunctional cortical maturation process of OCD at the network level. In this study, we showed the potential of an SVM model constructed using an individualized cortical morphology-based structural covariance network for predicting the initial response to SRI-based pharmacotherapy in OCD subjects with an accuracy of 89.0%. A more accurate prediction of the treatment response to the initial SRI-based pharmacotherapy combined with an individualized neuroimaging biomarker-based treatment regimen may lead to improvements in short-term symptomatology, long-term prognosis, and quality of life.

VI. REFERENCES

Alexander-Bloch A, Giedd JN, Bullmore E. Imaging structural co-variance between human brain regions. Nat Rev Neurosci 2013;14:322-36.

Alexander-Bloch A, Raznahan A, Bullmore E, Giedd J. The convergence of maturational change and structural covariance in human cortical networks. J Neurosci 2013;33:2889-99.

Anderson JS, Ferguson MA, Lopez-Larson M, Yurgelun-Todd D. Topographic maps of multisensory attention. Proc Natl Acad Sci U S A 2010;107:20110-4.

Andrews-Hanna JR, Reidler JS, Sepulcre J, Poulin R, Buckner RL. Functional-anatomic fractionation of the brain's default network. Neuron 2010;65:550-62.

Berney A, Leyton M, Gravel P, Sibon I, Sookman D, Rosa Neto P, Diksic M, Nakai A, Pinard G, Todorov C, Okazawa H, Blier P, Nordahl TE, Benkelfat C. Brain regional alpha-[11C]methyl-L-tryptophan trapping in medication-free patients with obsessive-compulsive disorder. Arch Gen Psychiatry 2011;68:732-41.

Binnewijzend MA, Adriaanse SM, Van der Flier WM, Teunissen CE, de Munck JC, Stam CJ, Scheltens P, van Berckel BN, Barkhof F, Wink AM. Brain network alterations in Alzheimer's disease measured by eigenvector centrality in fMRI are related to cognition and CSF biomarkers. Hum Brain Mapp 2014;35:2383-93.

Bruhl AB, Kaffenberger T, Herwig U. Serotonergic and noradrenergic modulation of emotion processing by single dose antidepressants. Neuropsychopharmacology 2010;35:521-33.

Bruss GS, Gruenberg AM, Goldstein RD, Barber JP. Hamilton Anxiety Rating Scale Interview guide: joint interview and test-retest methods for interrater reliability. Psychiatry Res 1994;53:191-202.

Bryan K, Leise T . The $25,000,000,000 Eigenvector: The Linear Algebra behind Google. SIAM Rev 2006;48:569-581.

Chen CH, Fiecas M, Gutierrez ED, Panizzon MS, Eyler LT, Vuoksimaa E, Thompson WK, Fennema-Notestine C, Hagler DJ Jr, Jernigan TL, Neale MC, Franz CE, Lyons MJ, Fischl B, Tsuang MT, Dale AM, Kremen WS. Genetic topography of brain morphology. Proc Natl Acad Sci U S A 2013;110:17089-94.

Chen CH, Gutierrez ED, Thompson W, Panizzon MS, Jernigan TL, Eyler LT, Fennema-Notestine C, Jak AJ, Neale MC, Franz CE, Lyons MJ, Grant MD, Fischl B, Seidman LJ, Tsuang MT, Kremen WS, Dale AM. Hierarchical genetic organization of human cortical surface area. Science 2012;335:1634-6.

Clarkson MJ, Cardoso MJ, Ridgway GR, Modat M, Leung KK, Rohrer JD, Fox NC, Ourselin S. A comparison of voxel and surface based cortical thickness estimation methods. Neuroimage 2011;57:856-865.

da Conceicao Costa DL, Shavitt RG, Castro Cesar RC, Joaquim MA, Borcato S, Valerio C, Miguel EC, Diniz JB. Can early improvement be an indicator of treatment response in obsessive-compulsive disorder? Implications for early-treatment decision-making. J Psychiatr Res 2013;47:1700-7.

Destrieux C, Fischl B, Dale A, Halgren E. Automatic parcellation of human cortical gyri and sulci using standard anatomical nomenclature. Neuroimage 2010;53:1-15.

Dold M, Aigner M, Lanzenberger R, Kasper S. Antipsychotic augmentation of serotonin reuptake inhibitors in treatment-resistant obsessive-compulsive disorder: a meta-analysis of double-blind, randomized, placebo-controlled trials. Int J Neuropsychopharmacol 2013;16:557-74.

Dosenbach NU, Nardos B, Cohen AL, Fair DA, Power JD, Church JA, Nelson SM, Wig GS, Vogel AC, Lessov-Schlaggar CN, Barnes KA, Dubis JW, Feczko E, Coalson RS, Pruett JR Jr, Barch DM, Petersen SE, Schlaggar BL. Prediction of individual brain maturity using fMRI. Science 2010;329:1358-61.

Fallucca E, MacMaster FP, Haddad J, Easter P, Dick R, May G, Stanley JA, Rix C, Rosenberg DR. Distinguishing between major depressive disorder and obsessive-compulsive disorder in children by measuring regional cortical thickness. Arch Gen Psychiatry 2011;68:527-33.

Farris SG, McLean CP, Van Meter PE, Simpson HB, Foa EB. Treatment response, symptom remission, and wellness in obsessive-compulsive disorder. J Clin Psychiatry 2013;74:685-90.

Fineberg NA, Pampaloni I, Pallanti S, Ipser J, Stein DJ. Sustained response versus relapse: the pharmacotherapeutic goal for obsessive-compulsive disorder. Int Clin Psychopharmacol 2007;22:313-22.

Fischl B, Dale AM. Measuring the thickness of the human cerebral cortex from magnetic resonance images. Proc Natl Acad Sci U S A 2000;97:11050-11055.

Fischl B, van der Kouwe A, Destrieux C, Halgren E, Segonne F, Salat DH, Busa E, Seidman LJ, Goldstein J, Kennedy D, Caviness V, Makris N, Rosen B, Dale AM. Automatically parcellating the human cerebral cortex. Cereb Cortex 2004;14:11-22.

Goodman WK, Price LH, Rasmussen SA, Mazure C, Fleischmann RL, Hill CL, Heninger GR, Charney DS. The Yale-Brown Obsessive Compulsive Scale. I. Development, use, and reliability. Arch Gen Psychiatry 1989;46:1006-11.

Gyurak A, Patenaude B, Korgaonkar MS, Grieve SM, Williams LM, Etkin A. Frontoparietal Activation During Response Inhibition Predicts Remission to Antidepressants in Patients with Major Depression. Biol Psychiatry 2015 (in press).

Hahn T, Kircher T, Straube B, Wittchen HU, Konrad C, Strohle A, Wittmann A, Pfleiderer B, Reif A, Arolt V, Lueken U. Predicting Treatment Response to Cognitive Behavioral Therapy in Panic Disorder With Agoraphobia by Integrating Local Neural Information. JAMA Psychiatry 2015;72:68-74.

Han JY, Kang DH, Gu BM, Jung WH, Choi JS, Choi CH, Jang JH, Kwon JS. Altered

brain activation in ventral frontal-striatal regions following a 16-week pharmacotherapy in unmedicated obsessive-compulsive disorder. J Korean Med Sci 2011;26:665-74.

He Y, Chen Z, Evans A. Structural insights into aberrant topological patterns of large-scale cortical networks in Alzheimer's disease. J Neurosci 2008;28:4756-66.

Henry ME, Lauriat TL, Lowen SB, Churchill JH, Hodgkinson CA, Goldman D, Renshaw PF. Effects of citalopram and escitalopram on fMRI response to affective stimuli in healthy volunteers selected by serotonin transporter gype. Psychiatry Res 2013;213:217-24.

Hoexter MQ, Miguel EC, Diniz JB, Shavitt RG, Busatto GF, Sato JR. Predicting obsessive-compulsive disorder severity combining neuroimaging and machine learning methods. J Affect Disord 2013;150:1213-6.

Hollander E. Obsessive-compulsive disorder: the hidden epidemic. J Clin Psychiatry 1997;58 Suppl 12:3-6.

Jouen AL, Ellmore TM, Madden CJ, Pallier C, Dominey PF, Ventre-Dominey J. Beyond the word and image: characteristics of a common meaning system for language and vision revealed by functional and structural imaging. Neuroimage 2015;106:72-85.

Koutsouleris N, Meisenzahl EM, Davatzikos C, Bottlender R, Frodl T, Scheuerecker J, Schmitt G, Zetzsche T, Decker P, Reiser M, Möller HJ, Gaser C.. Use of neuroanatomical pattern classification to identify subjects in at-risk mental states of

psychosis and predict disease transition. Arch Gen Psychiatry 2009;66:700-12.

Kremen WS, Fennema-Notestine C, Eyler LT, Panizzon MS, Chen CH, Franz CE, Lyons MJ, Thompson WK, Dale AM. Genetics of brain structure: contributions from the Vietnam Era Twin Study of Aging. Am J Med Genet B Neuropsychiatr Genet 2013;162b:751-61.

Leaver EE, Low KA, DiVacri A, Merla A, Fabiani M, Gratton G. The Devil Is in the Detail: Brain Dynamics in Preparation for a Global-Local Task. J Cogn Neurosci 2015:1-15.

Leroy F, Glasel H, Dubois J, Hertz-Pannier L, Thirion B, Mangin JF, Dehaene-Lambertz G. Early maturation of the linguistic dorsal pathway in human infants. J Neurosci 2011;31:1500-6.

Li F, Huang X, Tang W, Yang Y, Li B, Kemp GJ, Mechelli A, Gong Q. Multivariate pattern analysis of DTI reveals differential white matter in individuals with obsessive-compulsive disorder. Hum Brain Mapp 2014;35:2643-51.

Liang X, Zou Q, He Y, Yang Y. Topologically Reorganized Connectivity Architecture of Default-Mode, Executive-Control, and Salience Networks across Working Memory Task Loads. Cereb Cortex 2015 (in press).

Maslov S, Sneppen K. Specificity and stability in topology of protein networks. Science 2002;296:910-913.

Meyer M, Liem F, Hirsiger S, Jancke L, Hanggi J. Cortical surface area and cortical thickness demonstrate differential structural asymmetry in auditory-related areas of the human cortex. Cereb Cortex 2014;24:2541-52.

Muller MJ, Dragicevic A. Standardized rater training for the Hamilton Depression Rating Scale (HAMD-17) in psychiatric novices. J Affect Disord 2003;77:65-9.

Newman ME. Modularity and community structure in networks. Proc Natl Acad Sci U S A 2006;103:8577-8582.

Noble WS. What is a support vector machine? Nat Biotechnol 2006;24:1565-7.

Pauls DL, Abramovitch A, Rauch SL, Geller DA. Obsessive-compulsive disorder: an integrative genetic and neurobiological perspective. Nat Rev Neurosci 2014;15:410-24.

Robertson B, Wang L, Diaz MT, Aiello M, Gersing K, Beyer J, Mukundan S Jr, McCarthy G, Doraiswamy PM. Effect of bupropion extended release on negative emotion processing in major depressive disorder: a pilot functional magnetic resonance imaging study. J Clin Psychiatry 2007;68:261-7.

Rubinov M, Sporns O. Complex network measures of brain connectivity: uses and interpretations. Neuroimage 2010;52:1059-1069.

Ruscio AM, Stein DJ, Chiu WT, Kessler RC. The epidemiology of obsessive-compulsive disorder in the National Comorbidity Survey Replication. Mol Psychiatry

2010;15:53-63.

Seeley WW, Menon V, Schatzberg AF, Keller J, Glover GH, Kenna H, et al. Dissociable intrinsic connectivity networks for salience processing and executive control. J Neurosci 2007;27:2349-56.

Shaw P, Sharp W, Sudre G, Wharton A, Greenstein D, Raznahan A, Evans A, Chakravarty MM, Lerch JP, Rapoport J. Subcortical and cortical morphological anomalies as an endophenotype in obsessive-compulsive disorder. Mol Psychiatry 2015;20:224-31.

Shen Y, Yao J, Jiang X, Zhang L, Xu L, Feng R, Cai L, Liu J, Wang J, Chen W. Sub-hubs of baseline functional brain networks are related to early improvement following two-week pharmacological therapy for major depressive disorder. Hum Brain Mapp 2015 (in press).

Shim G, Park HY, Jang JH, Kim E, Park HY, Hwang JY, Kim SN, Jang GE, Kwon JS. What is the optimal dose of escitalopram for the treatment of obsessive-compulsive disorder? A naturalistic open-label study. Int Clin Psychopharmacol 2011;26:284-90.

Shin DJ, Jung WH, He Y, Wang J, Shim G, Byun MS, Jang JH, Kim SN, Lee TY, Park HY, Kwon JS. The effects of pharmacological treatment on functional brain connectome in obsessive-compulsive disorder. Biol Psychiatry 2014;75:606-14.

Shin G, Kim C. Neural correlates of cognitive style and flexible cognitive control. Neuroimage 2015;113:78-85.

Smith DV, Sip KE, Delgado MR. Functional connectivity with distinct neural networks tracks fluctuations in gain/loss framing susceptibility. Hum Brain Mapp (in press).

Song C, Schwarzkopf DS, Kanai R, Rees G. Neural population tuning links visual cortical anatomy to human visual perception. Neuron 2015;85:641-56.

Soriano-Mas C, Pujol J, Alonso P, Cardoner N, Menchon JM, Harrison BJ, Deus J, Vallejo J, Gaser C. Identifying patients with obsessive-compulsive disorder using whole-brain anatomy. Neuroimage 2007;35:1028-37.

Stein DJ, Koen N, Fineberg N, Fontenelle LF, Matsunaga H, Osser D, Simpson HB. A 2012 evidence-based algorithm for the pharmacotherapy for obsessive-compulsive disorder. Curr Psychiatry Rep 2012;14:211-9.

Teicher MH, Anderson CM, Ohashi K, Polcari A. Childhood maltreatment: altered network centrality of cingulate, precuneus, temporal pole and insula. Biol Psychiatry 2014;76:297-305.

Tomioka H, Yamagata B, Kawasaki S, Pu S, Iwanami A, Hirano J, Nakagome K, Mimura M. A longitudinal functional neuroimaging study in medication-naive depression after antidepressant treatment. PLoS One 2015;10:e0120828.

Uddin LQ. Salience processing and insular cortical function and dysfunction. Nat Rev Neurosci 2015;16:55-61.

Uehara T, Yamasaki T, Okamoto T, Koike T, Kan S, Miyauchi S, Kira J, Tobimatsu S. Efficiency of a "small-world" brain network depends on consciousness level: a resting-state FMRI study. Cereb Cortex 2014;24:1529-1539.

van den Heuvel MP, Sporns O, Collin G, Scheewe T, Mandl RC, Cahn W, Goni J, Hulshoff Pol HE, Kahn RS. Abnormal rich club organization and functional brain dynamics in schizophrenia. JAMA Psychiatry 2013;70:783-792.

Van Snellenberg JX, Slifstein M, Read C, Weber J, Thompson JL, Wager TD, Shohamy D, Abi-Dargham A, Smith EE. Dynamic shifts in brain network activation during supracapacity working memory task performance. Hum Brain Mapp 2015;36:1245-64.

van Waarde JA, Scholte HS, van Oudheusden LJ, Verwey B, Denys D, van Wingen GA. A functional MRI marker may predict the outcome of electroconvulsive therapy in severe and treatment-resistant depression. Mol Psychiatry 2015;20:609-14.

Wang L, Li K, Zhang Q, Zeng Y, Dai W, Su Y, Wang G, Tan Y, Jin Z, Yu X, Si T. Short-term effects of escitalopram on regional brain function in first-episode drug-naive patients with major depressive disorder assessed by resting-state functional magnetic resonance imaging. Psychol Med 2014;44:1417-26.

Watts DJ, Strogatz SH. Collective dynamics of 'small-world' networks. Nature 1998;393:440-442.

Wee CY, Yap PT, Shen D, Alzheimer's Disease Neuroimaging I. Prediction of

Alzheimer's disease and mild cognitive impairment using cortical morphological patterns. Hum Brain Mapp 2013;34:3411-25.

Xia M, Wang J, He Y. BrainNet Viewer: a network visualization tool for human brain connectomics. PLoS One 2013;8:e68910.

Yoo SY, Jang JH, Shin YW, Kim DJ, Park HJ, Moon WJ, Chung EC, Lee JM, Kim IY, Kim SI, Kwon JS. White matter abnormalities in drug-naive patients with obsessive-compulsive disorder: a Diffusion Tensor Study before and after citalopram treatment. Acta Psychiatr Scand 2007;116:211-9.

Zang Y, Jiang T, Lu Y, He Y, Tian L. Regional homogeneity approach to fMRI data analysis. Neuroimage 2004;22:394-400.

Zhang D, Liang B, Wu X, Wang Z, Xu P, Chang S, Liu B, Liu M, Huang R. Directionality of large-scale resting-state brain networks during eyes open and eyes closed conditions. Front Hum Neurosci 2015;9:81.

국문초록

강박증 환자에서 대뇌 피질 두께를 이용한 약물 치료반응 예측모델의 구축

윤 제 연

의학과 정신과학 전공

서울대학교 대학원

배경 및 목적: 강박증의 1 차 치료약물인 세로토닌 재흡수 억제제를 충분한 기간 동안 충분용량 사용한 경우에도, 약 40-60%의 강박증 환자들은 임상적으로 충분한 정도의 증상 호전에 도달하지 못하는 것으로 보고되어 왔다. 본 연구에서는 강박증 환자들의 구조적 뇌영상으로부터 대뇌 피질 표면 넓이 및 대뇌 피질 두께와 같은 특성의 개인내 공분산성 네트워크를 도출하여, 이러한 뇌과학적 특성이 개인별 수준에서 강박증 약물치료 반응군과 약물치료 비반응군을 신뢰롭게 구분할 수 있는 생물학적 마커로서 기계학습을 이용한 맞춤의학에 적용될 수 있는 가능성을 탐색하고자 하였다.

방법: 최근 4 주 이상의 기간 동안 항강박증 약물 투여력이 없는 56 명의 강박증 환자들 및 이들과 동일한 기간 동안 모집된 75 명의 정상대조군에 대하여 T1 신호강조 뇌영상을 촬영하고 임상평가를 시행한 후, 강박증 환자들에게는 서울대학교병원 강박증클리닉 외래에서 에스시탈로프람 등을 중심으로 한 항강박증 약물치료를 시행하였다. 이와 같이 4 개월이 경과한 후, 강박증 환자들은 치료 시작 시점에 Yale-Brown Obsessive Compulsive Scale 을 이용하 측정한 강박증상 심각도와 비교하여 치료 후 강박증상 심각도가 완화된 정도에 따라 강박증 치료반응군(OCD-R, *N=25*; ≥*35%* improvement) 혹은 강박증 치료비반응군(OCD-NR, *N=31*; <*35%* improvement) 으로 나누어졌다. 대뇌 피질표면넓이의 개인내 공분산 네트워크 및 대뇌 피질두께의 개인내 공분산 네트워크를 구한 후, 모든 회기의 leave-one-out group-comparison 에서 통계적으로 유의한 그룹간 차이를 나타내 공분산 요소들을 서포트 벡터 머신의 모델 구성요소로 사용한 기계학습 실험을 시행하였다.

결과: 배외측전전두피질의 대뇌피질두께와 쐐기앞소엽의 대뇌피질두께 사이의 개인내 공분산요소 및, 앞섬엽의 대뇌피질표면넓이와 두정엽내고랑의 대뇌피질표면넓이의 개인내 공분산요소, 그리고 실비안열 주변뇌부위들의 대뇌피질기반 개인내 공분산요소를 포함한 총 12 개의 대뇌피질기반 개인내 공분산네트워크 요소들을 이용하여 구축된 기계학습 모델은 강박증 환자의 4 개월 후 치료반응을 89.0% 의 평균정확도(평균민감도 88.4%, 평균특이도 90.1%)로 예측하였으며, 이로부터 보다 넓은 뇌부위들 사이의 대뇌피질기반 개인내 공분산네트워크 요소들을 포함하여 구축된 기계학습 모델은 강박증 환자들을 정상대조군으로부터 90.7-95.6%의 평균정확도 (평균민감도 90.8-96.2%, 평균특이도 91.1-95.0%)로 구분할 수 있었다.

결론: 본 연구는 대뇌피질의 비정상적인 발달 및 성숙과정의 경로를 반영하는 대뇌피질기반 개인내 공분산네트워크 요소들이 강박증 환자에서 세로토닌 재흡수 억제제를 사용한 약물치료에 대한 초기 치료반응의 정도를 효과적으로 예측할 수 있는 잠재적 생물학적 마커로서 기능할 가능성을 시사한다.

주요어: 강박증; 세로토닌 재흡수 억제제; 치료반응; 대뇌피질기반 공분산 네트워크; 기계학습; 생물학적 마커

학번: 2012-31126